Reac Kinet Mech Cat (2015) 114:571–582
DOI 10.1007/s11144-014-0805-0

Copper doped K-birnessite as an efficient catalyst for the synthesis of 2-aryl benzimidazoles

Bilge Eren · Huseyin Gumus

Received: 21 July 2014 / Accepted: 31 October 2014 / Published online: 15 November 2014

Abstract In this study, an efficient and highly selective synthesis of 2-aryl benzimidazoles from the reaction of *o*-phenylenediamine and aromatic aldehydes in the presence of birnessite type copper doped manganese oxide (BCM) is reported. BCM was synthesized by the one-step hydrothermal method. Recycling of BCM up to five runs was investigated with appreciable yield and selectivity of the products. The best overall yields and selectivities were obtained in methanol. The crystal structure and thermal stability of BCM are characterized by using XRD, IR and thermal analysis techniques. The acid sites of BCM were investigated by IR using pyridine as a molecular probe. The improved catalytic activity observed in the BCM catalyst was associated to a high lattice oxygen mobility and availability due to the formation of Cu–O–Mn bridges.

Keywords Benzimidazole · Birnessite · Cu doped birnessite · XRD

Introduction

The use of large volumes of volatile hazardous organic solvents and toxic metal catalysts in industrial processes poses a serious threat to the environment. There is an urgent need to develop alternative solvents and technologies due to pressure from governmental organizations and other regulatory bodies to protect the environment. Therefore, the search for finding a cost effective, mild and simple selective protocol especially using heterogeneous catalysts for the synthesis of organic compounds is still important.

Recent advances in nanoscience and nanotechnology have also led to the development of an efficient synthesis of bioactive compounds using nanoparticles in

B. Eren (✉) · H. Gumus
Department of Chemistry, Faculty of Science and Arts, Bilecik Seyh Edebali University, 11210 Bilecik, Turkey
e-mail: bilge.eren@bilecik.edu.tr

an ecologically and economically favorable way which is a great challenge in modern chemistry. The benzimidazole moiety is a structural isostere of naturally occurring nucleotides; hence, it has been a useful intermediate in the development of molecules of pharmaceutical and biological interests [1–3]. There are several methods for the synthesis of benzimidazole derivatives in the literature [4–11]. It is common to form benzimidazoles through the cyclocondensation of carboxylic acids or their derivatives with *o*-phenylenediamines under harsh dehydrating conditions [4–7]. In the presence of oxidants such as H_2O_2 [8], perborate [9], or cobalt oxide [10], aldehydes could also be transferred into benzimidazoles. In these kinds of reactions, directly employing the condensation–aromatization reaction of *o*-phenylenediamines and aldehydes gives a complex mixture such as 1,2-disubstituted benzimidazoles, bis-anil and dihydrobenzimidazoles as the main side products [11].

Manganese oxides exhibit considerable activity in oxidation–reduction reactions due to the presence of manganese ions with different oxidation states [12–14]. The high activity of manganese oxides was explained in terms of the characteristics of the oxygen species [15, 16]. These redox capabilities of these oxides can be enhanced when other metals are combined [17–20]. The improved catalytic properties observed in these materials were correlated with an enhanced lattice oxygen mobility and reactivity due to the interaction of the metal cation with the manganese oxide structure [17–23]. The modification of manganese oxides by the presence of Cu^{2+} has been postulated as a good alternative to improve their catalytic activity for catalytic oxidation reactions [20–23]. The Cu–Mn oxides are important industrially as a versatile and effective oxidation catalysts [20–23]. In these processes, the reversible electron transfer along the Cu–O–Mn bridge supposes the reduction and re-oxidation of the Cu^{2+} together with the Mn^{4+} of the oxide structure.

The selectivity in forming 1,2-diaryl benzimidazole and 2-aryl benzimidazole has high interest in the literature studies [24–33]. In the literature, there are more methods for synthesizing 1,2-diaryl benzimidazoles [24–30] compared to preparing 2-aryl benzimidazoles with ideal selectivity [31–33]. A careful analysis of the existing literature indicates that not many studies have been conducted at understanding the synthesis of benzimidazole derivatives by the condensation of *o*-phenylenediamine (*o*–PD) and aromatic aldehydes in different solvents using copper modified manganese oxides as a catalyst. Taking into account this background, we report an easy and efficient procedure for the selective synthesis of 2-aryl benzimidazoles catalyzed by the birnessite type copper doped manganese oxide (BCM). In this study, BCM was synthesized by a one-step hydrothermal method. This process is environmentally benign, easy to manipulate and can be scaled up further for industrial processes.

Experimental

Materials and sample preparation

All chemicals and solvents were obtained from Aldrich and Merck and used without further purification. Column chromatographic separations were carried out on silica gel 60–120 mesh size.

BCM was prepared by the oxidation of $Mn(NO_3)_2$ with H_2O_2 in KOH solutions in the presence of $Cu(NO_3)_2$. Accordingly, first 2 M H_2O_2 and 0.6 M KOH solutions were mixed and stirred in glass beaker. The molar ratio of $Cu(NO_3)_2$/$Mn(NO_3)_2$ was adjusted to 0.10. Immediately after that, manganese-copper solution was poured into the mixture. After the completion of bubble formation, the black precipitate was filtered. The obtained soil was put into the Teflon lined autoclave and waited at 130 °C for 16 h in 2 M KOH solution. The obtained grey precipitate was filtered and washed with deionized water until to obtain neutralization.

Characterization techniques

FTIR spectra of the samples were recorded in the region 4,000–450 cm^{-1} on a Spectrum-100 FTIR spectrometer. The TG and DTG curves were obtained using a Seiko Exstar 7000 thermal analyzer under air atmosphere. The XRD analysis data from the samples were collected using a Rigaku, Miniflex ZD13113 (Japan) diffractometer with Cu K_α radiation (Ni-filtered).

Surface acidity study

The sample was dried in a hot air oven for 24 h at 120 °C before pyridine treatment for IR measurements. The sample (50 mg) was poured loosely into a sample cup. The loosely filled sample was brought in contact with pyridine (0.1 cm^3) directly. Then the sample cup was kept in a hot air oven at 100 °C for 1 h to remove physisorbed pyridine. After cooling down to room temperature and adsorption of pyridine, the sample adsorbed pyridine was evacuated for 20 min at several temperatures (120–500 °C). Specimens for measurement were prepared by mixing 0.9 mg of the sample powder with 70 mg of KBr and pressing the mixture into a pellet.

Catalytic activity study

The catalytic activity of BCM was investigated in the condensation reaction between *o*–PD and aldehyde. In a typical procedure, a mixture of *o*–PD (2 mmol), aldehyde (2.2 mmol), solvent (5 ml) and BCM (70 mg) were taken in a 50 ml flask at room temperature. The progress of the reaction was monitored periodically by analyzing the reaction mixture by thin layer chromatography using a mixture of n-hexane and ethyl acetate in 4:1 ratio. After the completion of the reaction, the reaction mixture was filtered by a PET syringe filter to recover the solid catalyst, and the filtrate was poured into 100 mL water containing crushed ice.

All of the compounds are known compounds. They were identified from their ^1H NMR spectroscopic data and by comparing their mps with those reported in the literature [34, 35].

2-Phenylbenzimidazole (**1**) m.p. 292–293 °C (lit., [34] 290–293 °C); IR (υ, cm^{-1}): 3150, 5055, 1600, 1545, 1310, 1270; ^1H NMR (400 MHz, DMSO-d_6): δ 7.15–7.20 (m, 2H), 7.39–7.70 (m, 5H), 8.10–8.20 (m, 2H) 12.90 (bs, 1H).

2-(4-Methylphenyl)benzimidazole (**2**) m.p. 274–276 °C (lit., [34] 269–273 °C); IR (υ, cm^{-1}): 3120, 3080, 2923, 1615, 1575, 1310, 1273; ^1H NMR (400 MHz,

DMSO-d_6): δ 2.33 (s, 3H), 7.15–7.25 (m, 2H), 7.32 (d, 2H), 7.50 (d, 1H), 7.62 (d, 1H), 8.08 (d, 2H) 12.85 (bs, 1H).

2-(2-Hydroxyphenyl)benzimidazole (**3**) m.p. 237–238 °C (lit., [34] 240–242 °C); IR (υ, cm^{-1}): 3250, 3083, 1665, 1600, 1310, 1273; ^{1}H NMR (400 MHz, DMSO-d_6): δ 7.00–7.04 (m, 2H), 7.25 (s, 2H), 7.67 (bs, 2H), 7.35 (t, 1H), 8.04 (d, 2H), 13.12 (s, 2H).

2-(4-Chlorophenyl)benzimidazole (**4**) m.p. 289–290 °C (lit., [35] 288–291 °C); IR (υ, cm^{-1}): 3055, 1602, 1578, 1320, 1275; ^{1}H NMR (400 MHz, DMSO-d_6): δ 7.18 (dd, 2H), 7.55 (bs, 2H), 7.63 (d, 2H), 8.20 (d, 2H), 12.98 (bs, 1H).

2-(4-Nitrophenyl)benzimidazole (**5**) m.p. 313–316 °C (lit., [35] 308–310 °C); IR (υ, cm^{-1}): 3033, 1610, 1520, 1434, 1320, 730; ^{1}H NMR (400 MHz, DMSO-d_6): δ 7.00–7.13 (m, 2H), 7.58 (dd, 2H), 7.93 (d, 2H), 8.21 (d, 2H), 12.93 (bs, 1H).

Reusability of catalyst

After the completion of the reaction, reaction mixture was filtered and the catalyst was washed with ethanol (3 times) and then kept for drying at 100 °C for 2 h, after which the catalyst was reused for next cycle. The catalyst reusability was checked for the first step of oxidation and also for the sequential protocol.

Results and discussion

Characterization of BCM

Fig. 1 shows XRD patterns of K-birnessite and BCM prepared by using K-birnessite. Fig. 1a shows four major XRD peaks at $2\theta = 12.58°$ (0.722 nm), 25.08° (0.362 nm), 37.08° (0.245 nm), and 65.67° (0.141 nm), which are the typical reflections of layered birnessite-type manganese oxides [36–38]. No other peaks are present in XRD pattern of K-birnessite, indicating that it is single phased hexagonal birnessite. BCM exhibited the same XRD characteristics as the K-birnessite (Fig. 1b). Also, no additional peaks of CuO were observed, suggesting that the doping of copper ions into the lamellar birnessite did not affect the crystal structure, and no second phase was introduced. However, the peak intensity of BCM slightly decreased, and their full width at half-maximum slightly increased, indicating a decrease in particle size and crystallinity. The lattices of the birnessites consist of negatively charged oxide layers and positively charged interlayers incorporating cations and water molecules. Structural defects are created to maintain the charge balance and accommodate the size difference between Cu^{2+} and Mn^{2+}. No structure defects are expected when Cu^{2+} replaces Mn^{2+}, because Cu^{2+} (0.71 nm) [39] has an identical ion radius and the same charge as Mn^{2+} (0.83 nm) [39]. The incorporation of Cu^{2+} within the birnessite structure involves exchange with potassium and also removal of Mn^{2+}.

The IR spectra of K-birnessite and BCM samples in the range from 1,700 to 450 cm^{-1} are shown in Fig. 2. The absorption band at 1,630 cm^{-1} is caused by disordered H_2O in the interlayer space of K-birnessite or adsorbed H_2O. The birnessite-type structure is characterized by two prominent bands at around 511 and

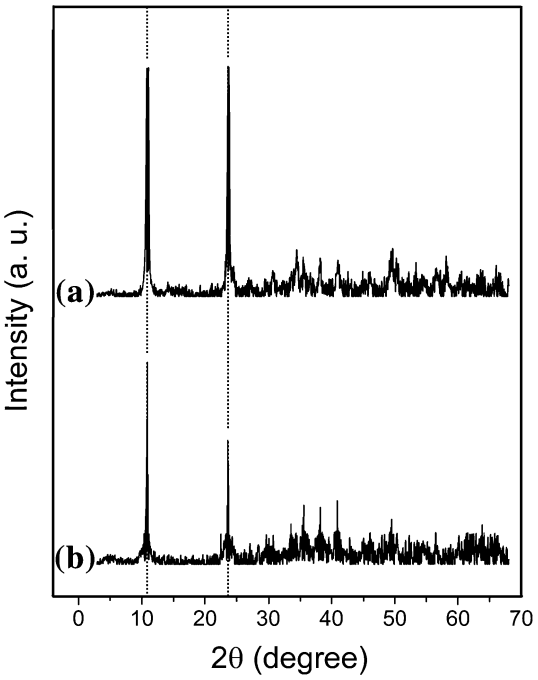

Fig. 1 XRD patterns of K-birnessite (*a*) and BCM (*b*)

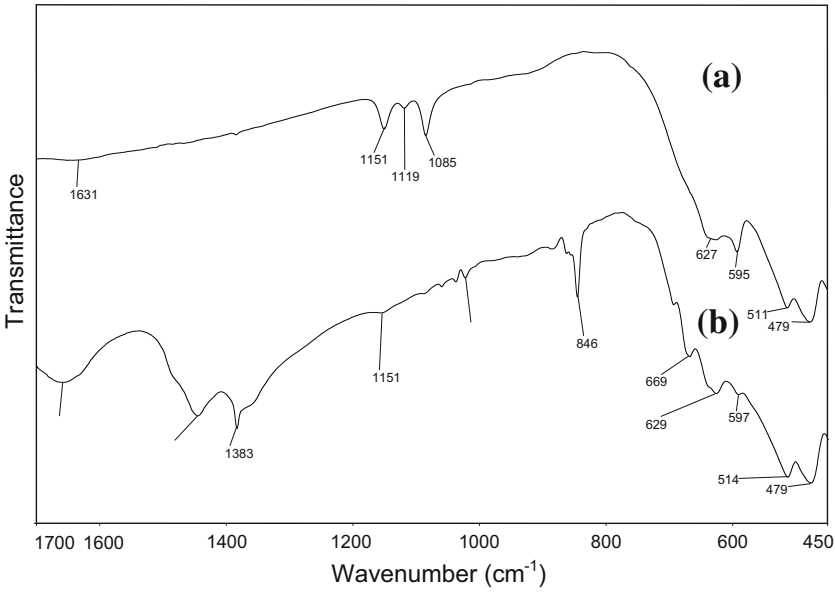

Fig. 2 FT-IR spectra of K-birnessite (*a*) and BCM (*b*) in the range of 450–1,700 cm^{-1}

479 cm^{-1} [37, 38, 40]. The band at 511 cm^{-1} is related to the asymmetric stretching vibrations of MnO_6 (Mn^{4+}/Mn^{3+}) octahedra involving the displacement of manganese ions in direction perpendicular to the MnO_4 plane. The peak at 479 cm^{-1} is attributed to the Mn–O–Mn bending mode. The band located at 629 cm^{-1} presented Mn_2O_3 phase. The positions of these bands were changed with the Cu^{2+} doping process.After the Cu^{2+} doping process, the band at 511 cm^{-1} for the K-birnessite sample shifted to 514 cm^{-1} for BCM sample. Therefore, the shifting of these bands towards the longer wavelengths was considered as the indicator of doped Cu^{2+}, and also accepted as evidence for the decrease of the surface Mn–O bond strength. The increase of the width of the bands in the range of 479–629 cm^{-1} in BCM spectrum, i.e. the growth in its integral intensity was another confirmation of the fact that the ionic feature Mn–O bond was growing stronger. These results indicated that Cu^{2+} doping process influenced the mobility of the reactive oxygen. The intensity of the Mn–O band was proportional to the content of active oxygen [41]. The BCM sample has weaker Mn–O bond in the Mn–O–Cu bridge, and stronger mobility and reactivity of the active oxygen species due to the high electronegativity of Cu. The vibrations above 800 cm^{-1} demonstrate the existence of the OH bonds, including γ-OH (1,085 cm^{-1}), δ-2-OH (1,119 cm^{-1}) and δ-1-OH (1,151 cm^{-1}) [40]. In this region, the transmittance peaks of the K-birnessite sample are much stronger than those of the BCM sample. The introduction of Cu^{2+} affected the interaction between Mn and OH or O. As a result, these bands disappeared. Some Cu^{2+} interacted with O atom to yield Cu–O–Mn like bonds leading to an appearance of novel band of OH group at around 846 cm^{-1}. The intensity of the absorption band at 595 cm^{-1} decreased after Cu^{2+} doping process. The sharpness of the Mn–O vibration bands for BCM are lower than that of K-birnessite. This suggests that the crystallinity of the BCM is weaker than that of K-birnessite.

TG, DTA and DTG curves for K-birnessite and BCM samples were shown in Fig. 3a and 3b. The curve related to K-birnessite exhibited mass losses by 10.8 and 5.6 % in the temperature ranges 30–200 °C and 200–1,000 °C, respectively (Fig. 3a). The K-birnessite sample showed an initial weight at around 167 °C with weight loss of 4.5 %, due to water molecules present in the layer structure. The mass loss of 0.2 % between 250 and 445 °C was due to the loss of oxygen atoms from the octahedral layer framework in relation to the partial reduction of Mn^{4+} to Mn^{3+} [42–44], whereas the weight gain centered at 510 °C was attributed to subsequent oxidation of some Mn^{3+} to Mn^{4+} [42–44]. The last mass loss of 4.9 % observed in the range of 853–931 °C implies oxygen depletion from the structure of the Mn_2O_3 and its subsequent decomposition to Mn_3O_4 [42–44]. The DTG profile of BCM was similar to K-birnessite, but weight losses occurred at lower temperature ranges (Fig. 3b). The dehydration of BCM occurred with a mass loss of 17.6 % whereas this same process happened with a mass loss of 16.4 % for K-birnessite in the temperature range of 30–1,000 °C. The BCM catalyst showed a first weight loss around 165 °C with a weight loss value of 13.9 % due to the loss of water molecules present in BCM and the last weight loss in the temperature range of 640–796 °C with a weight loss value of 3.7 %, due transformation of MnO_2 phase into Mn_2O_3 and Mn_3O_4 phases [42–44].

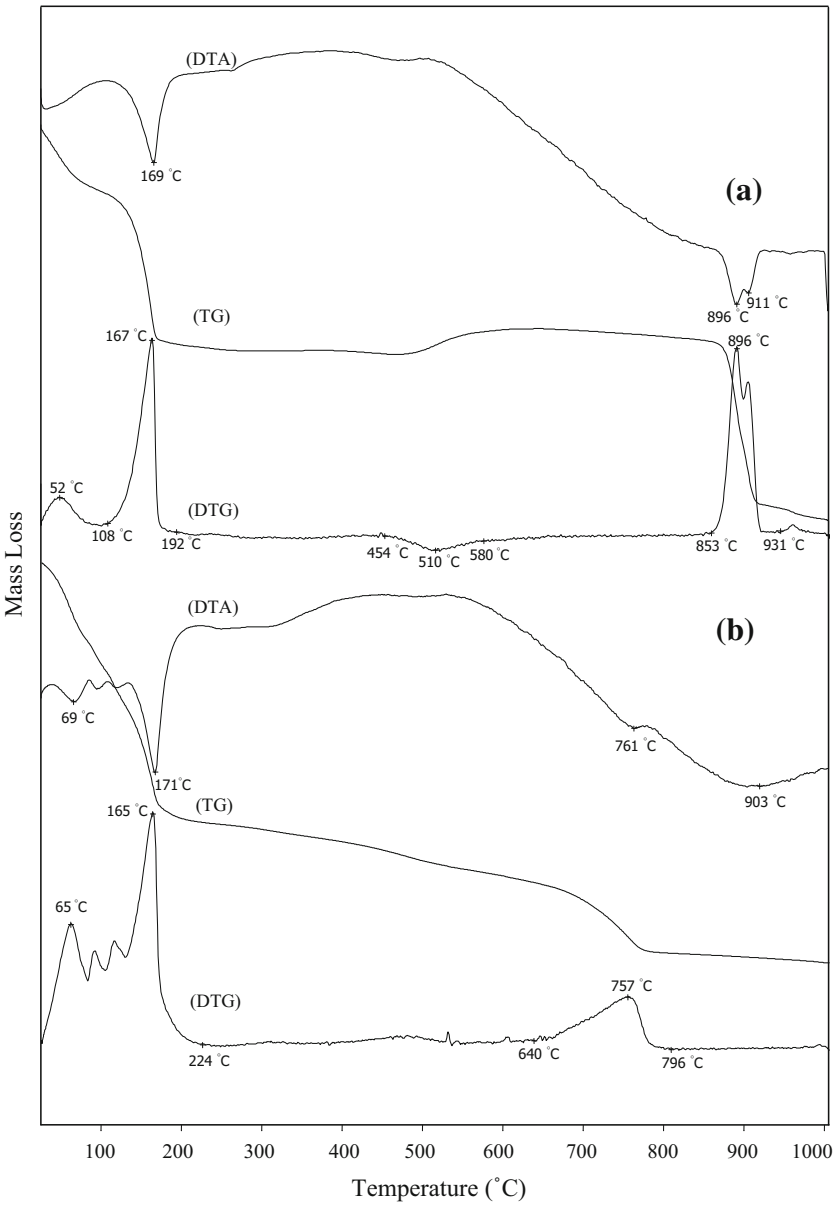

Fig. 3 DTA, TG and DTG curves of K-birnessite (*a*) and BCM (*b*) samples

Surface acidity of BCM

The IR spectra in the spectral region 1,400 and 1,700 cm^{-1} after pyridine treatment for 20 mins of pyridine adsorbed on BCM is presented in Fig. 4. The IR absorption bands were assigned according to literature [45–47]. The IR spectra of the adsorbed

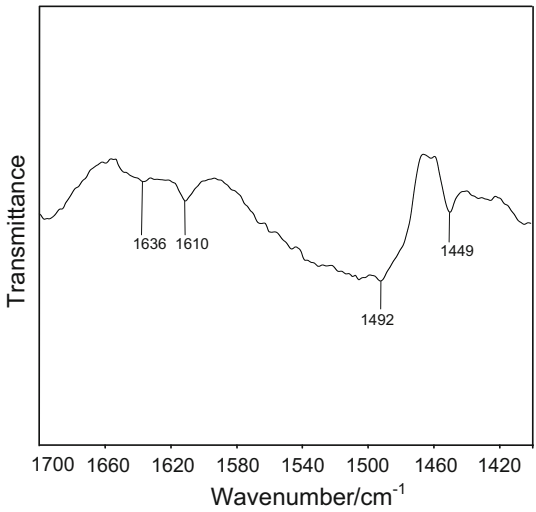

Fig. 4 Desorption of pyridine from BCM at 120 °C

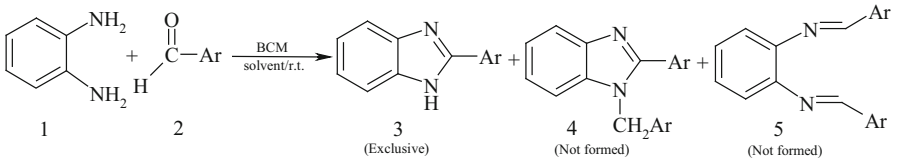

Scheme 1 Possible products for the direct condensation of *o*–PD with aryl aldehydes

pyridine on BCM showed absorption bands at 1636, 1610, 1492, and 1449 cm^{-1} (Fig. 4). For the BCM sample at 120 °C (Fig. 4), the main vibration bands arising from the adsorbed pyridine are those bound on Lewis acid sites which are observed at 1,449 and 1,610 cm^{-1}. The strong band at 1,490 cm^{-1} is attributed to pyridine associated with both Lewis and Brønsted acid sites. The band at 1,636 cm^{-1} is due to the vibration of interlayer water molecules in BCM sample. From these results, it is found that acid sites of BCM are predominantly Lewis acidic in nature. This means that the metal cation acts as electron pair accepters and can potentially act as Lewis acid catalyst.

Catalytic activity study

The reaction between *o*–PD and benzaldehyde (BA) was selected for the synthesis of benzimidazole as a model reaction for optimizing the reaction conditions in various solvents at room temperature (Scheme 1). The obtained results are summarized in Table 1. It was found that as the amount of BCM was increased from 0 to 100 mg yield of the benzimidazole also increased. Among various solvents like THF, water, isopropanol, DMF, acetonitrile, ethanol and methanol used for this transformation, ethanol (87 %) and methanol (95 %) exhibited almost

Table 1 Optimization of benzimidazole synthesis using *o*–PD and BA

Entry	Amount of BCM (mg)	Solvent	Temperature	Time (h)	% Yield of 3
1	0	Methanol	R.T.	2	No yield
2	20	Methanol	R.T.	2	54
3	40	Methanol	R.T.	2	58
4	60	Methanol	R.T.	2	71
5	70	Methanol	R.T.	2	73
6	80	Methanol	R.T.	2	75
7	100	Methanol	R.T.	2	75
8	70	Ethanol	R.T.	2	87
9	70	Isopropanol	R.T.	3	68
10	70	Methanol	R.T.	3	95
11	70	THF	R.T.	3	18
12	70	H_2O	R.T.	3	No yield
13	70	DMF	R.T.	3	15
14	70	Acetonitrile	R.T.	3	45

Reaction conditions: *o*–PD (2 mmol); BA (2.2 mmol) in the presence of BCM (70 mg)

% Yields refer to the isolated yield of the compounds after chromatographic separation and characterized by ^{1}H spectral data

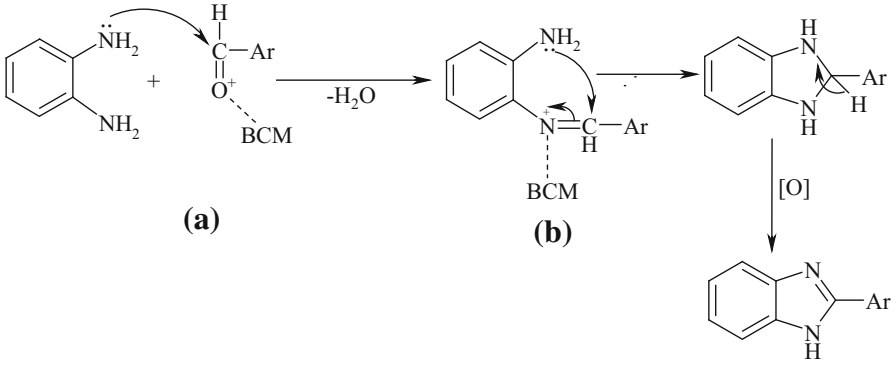

Scheme 2 Proposed mechanism for the synthesis of benzimidazoles

the same activity, DMF and THF showed poor activity (15 and 18 %, respectively). A compromise between polarity and a little hydrophobicity might result in the best performance for methanol.

After establishing the optimized reaction conditions, we attempted to generalize the designed protocol using various aldehydes. The results revealed that the electronic nature of the substituent on the phenyl ring had a significant effect on the yield and selectivity (Table 2). Benzaldehydes with electron donating groups produced the corresponding benzimidazoles in good to excellent yields (entries 2 and 3). Benzaldehydes bearing electron withdrawing groups (entries 4 and 5) gave

Table 2 Reactions between *o*–PD and various substituted aldehydes

Entry	Ar	Time (h)	Temperature	% Yield of 3
1	$-C_6H_5$	3	R.T.	95
2	$4\text{-}CH_3C_6H_5$	2.5	R.T.	95
3	$2\text{-}OHC_6H_5$	2	R.T.	94
4	$4\text{-}ClC_6H_5$	6	R.T.	75
5	$4\text{-}NO_2C_6H_5$	10	R.T.	83

Reaction conditions: *o*–PD (2 mmol); aldehyde (2.2 mmol) in the presence of BCM (70 mg) in methanol as solvent

% Yields refer to the isolated yield of the compounds after chromatographic separation and characterized by ^1H spectral data

Table 3 Studies on the reuse of BCM in the reaction of *o*–PD and benzaldehyde

Entry	Cycle number	% Yield of 3
1	1	73
2	2	68
3	3	64
4	4	55
5	5	50

% Yield refer to the isolated yield of 3

the slightly lower yields. To account for the facile formation of benzimidazoles, the following mechanism (Scheme 2) is proposed. According to this mechanism, the Lewis acidic sites of BCM react with carbonyl oxygen of aldehyde (a). Subsequent condensation of (a) with *o*–PD leads to the formation of imine species (b). This resulting imine further reacts with another $-NH_2$ group of *o*–PD resulting in the formation of dihydroimidazole, which subsequently undergoes aromatization under the oxidative conditions to give the benzimidazol.

To the best of our knowledge, these reactions have never been reported by using BCM. The catalytic activity of the recovered catalyst was examined as shown in Table 3. At the end of the reaction, the catalyst was filtered off, washed with mixture of hot ethanol and water, dried at 100 °C for 3 h, and reused as such for subsequent experiments (up to five cycles) under similar reaction conditions. It was noticed that yields of the product remained comparable in these experiments (Table 3), and thereby pointing the recyclability and reusability of the catalyst without any significant loss in catalytic activity.

Conclusion

BCM was used as a new selective Lewis acid catalyst for the synthesis of 2-substituted benzimidazoles from the reaction of aldehydes with *o*–PD. The catalyst is highly active, stable, and could be reused several times without much loss

of its activity. The heterogeneous nature and high acidity of the catalyst make the preparation of benzimidazoles simple, convenient, and practical. As this catalyst is highly active, this could also be used for several acid-catalyzed organic transformations and could replace the existing homogenous catalysts which are hazardous and currently being used in the industry. The developed process found to be excellent both in terms of yield, selectivity and time. The method overcomes the earlier disadvantages like corrosiveness, expensive process, waste generation and the use of ligand or additives. The yields of the products varied in the range of 14–70 % depending on the aldehyde used for the reaction. The vibrations of the Mn–O bond on the surface of K-birnessite and BCM samples indicated the presence of active oxygen. The catalyst BCM was recovered quantitatively by a simple filtration and reused with consistent activity even after the fifth cycle. The nature and position of substitution on the aryl ring did not make any much different in reactivity. The atomic absorption spectroscopy of the filtrate confirmed that no leaching of manganese or copper occurred during the reaction providing the evidence for the heterogeneous nature of the catalyst. These results make the process more attractive and interesting with respect to the economy of the process and simplicity.

Acknowledgments We would like to thank reviewers for their remarks and corrections of the manuscript.

References

1. Jadhav GR, Shaikh MU, Kale RP, Gill CH (2009) Chin Chem Lett 20:292–295
2. Chari MA, Kenawy SE, Al-Deyab SS, Subba Reddy BV, Vinu A (2010) Tetrahedron Lett 51:5195–5199
3. Shelkar R, Sarode S, Sarode J (2013) Tetrahedron Lett 54:6986–6990
4. Hasan M, Munawar S, Khan N, Maqbool Z (1998) Turk J Chem 22:367–371
5. Alinezhad H, Salehian F, Biparva P (2012) Synth Commun 42:102–108
6. Shingalapur RV, Hosamani KM (2010) Catal Lett 137:63–68
7. Taha MAM, Chin J (2005) Chem Soc 52:137–140
8. Duan LP, Li Q, Wu NB, Xu DF, Zhang HB (2014) Chin Chem Lett 25:155–158
9. Yuan J, Zhao Z, Zhu W, Li H, Qian X, Xu Y (2013) Tetrahedron 69:7026–7030
10. Chari MA, Shobha D, Sasaki T (2011) Tetrahedron Lett 52:5575–5580
11. Paul S, Basu B (2012) Tetrahedron Lett 32:4130–4133
12. Deng QF, Ren TZ, Yuan ZY (2013) Reac Kinet Mech Cat 108:507–518
13. D'alessandro O, Thomas HJ, Sambeth JE (2012) Reac Kinet Mech Cat 107:295–309
14. Kunkalekar RK, Salker AV (2012) Reac Kinet Mech Cat 106:395–405
15. Fakhreia A, Sagheer A, Zaki MI (2004) Microporous Mesoporous Mat 67:43–52
16. Cai LN, Guo Y, Lu AH, Branton P, Li WC (2012) J Mol Catal A 360:35–41
17. Kunkalekar RK, Salker AV (2013) Reac Kinet Mech Cat 108:173–182
18. Curia V, Sambeth J, Gambaro L (2012) Reac Kinet Mech Cat 106:165–176
19. Jothiramalingam R, Viswanathan B, Varadarajan TK (2006) J Mol Catal A 252:49–55
20. Zhı K, Lıu Q, Zhang Y, He S, He R (2010) J Fuel Chem Technol 38:445–451
21. Kondrat SA, Davies TE, Zu Z, Boldrin P, Bartley JK, Carley AF, Taylor SH, Rosseinsky MJ, Hutchings GJ (2011) J Catal 281:279–289
22. Li F, Zhang L, Evans DG, Duan X (2004) Colloids Surf A 244:169–177
23. Patel A, Shukla P, Chen J, Rufford TE, Rudolph V, Zhu Z (2013) Catal Today 212:38–44
24. Bandyopadhyay P, Sathe M, Prasad GK, Sharma P, Kaushik MP (2011) J Mol Catal 341:77–82
25. Yu H, Zhang MS, Cui LR (2012) Chin Chem Lett 23:573–575

26. Ghosh P, Mandal A (2011) Catal Commun 12:744–747
27. Paul S, Basu B (2012) Tetrahedron Lett 53:4130–4133
28. Salehi P, Dabiri M, Zolfigol MA, Otokesh S, Baghbanzadeh M (2006) Tetrahedron Lett 47:2557–2560
29. Pramanik A, Roy R, Khan S, Ghatak A, Bhar S (2014) Tetrahedron Lett 55:1771–1777
30. Varala R, Nasreen A, Enugala R, Adapa SR (2007) Tetrahedron Lett 48:69–72
31. Mukhopadhyay C, Tapaswi K (2008) Catal Commun 9:2392–2394
32. Trivedi R, De SK, Gibbs RA (2006) J Mol Catal 245:8–11
33. Rekha M, Hamza A, Venugopal BR, Nagaraju N (2012) Chin J Catal 33:439–446
34. Behbahani FK, Lotfi A (2013) Eur Chem Bull 2:694–697
35. Xiangming H, Huiqiang M, Yulu W (2007) Arkivoc (xiii):150–154
36. Atkins AL, Shaw S, Peacock CL (2014) Geochim Cosmochim Acta 144:109–125
37. Yin H, Liu F, Feng X, Liu M, Tan W, Qui G (2011) J Hazard Mater 196:318–326
38. Eren E, Guney M, Eren B, Gumus H (2013) Appl Catal B 132–133:370–378
39. Yang J, Wang B, Cao J, Han D, Feng B, Wei M, Fan L, Kou C, Liu Q, Wang T (2013) J Alloy Compd 574:240–245
40. Li F, Wu J, Qin Q, Li Z, Huang X (2010) J Alloy Compd 492:339–346
41. Cui M, Jang M, Na S, Lee S, Khim J (2013) J Environ Manag 115:235–240
42. Liu L, Feng Q, Yanagisawa K, Bignall G, Hashida T (2002) J Mater Sci 37:1315–1320
43. Malankar H, Umare SS, Singh K, Sharma M (2010) J Solid State Electrochem Room 14:71–82
44. Gaillot AC, Lanson B, Drits VA (2005) Chem Mater 17:2959–2975
45. Eren B, Erdogan G (2012) Reac Kinet Mech Cat 107:333–344
46. Shimizu K, Higuchi T, Takasugi E, Hatamachi T, Kodama T, Satsuma A (2008) J Mol Catal A 284:89–96
47. Figueiredo FCA, Jordão E, Landers R, Carvalho WA (2009) Appl Catal A 371:131–141